Camera Calibration from a Single Night Sky Image

Andreas Klaus*, Joachim Bauer and
Konrad Karner
VRVis Research Center
Graz, Austria

Pierre Elbischger, Roland Perko and
Horst Bischof
Institute for Computer Graphics and Vision
Graz, Austria

Abstract

We present a simple and universal camera calibration method. Instead of extensive setups we are exploiting the accurate angular positions of fixed stars. High precision is achieved by compensating the interfering error sources. Our approach uses a star catalog and requires a single input image only. No additional user input information such as focal length, exposure date or position is required. Fully automatic processing and fast convergence is achieved by performing three consecutive steps. First, a star segmentation and centroid finding algorithm extracts the sub-pixel positions of the luminaries. Second, an initial solution for the most essential parameters is determined by combinatorial analysis. Finally, the Levenberg-Marquardt algorithm is applied to solve the resulting non-linear system. Experimental results with several digital consumer cameras demonstrate high robustness and accuracy. The introduced method is advisable for applications where large calibration targets are required.

1. Introduction

Camera calibration is a fundamental task in computer vision and establishes the transformation between object and image space. In most cases a simple projective transformation is not sufficient in terms of accuracy because of lens distortion. Therefore additional parameters for the used lens distortion model have to be estimated. Once the calculated distortion parameters are known, distortion correction can be accomplished.

Camera calibration methods can be classified into two basic categories [13]: Self calibration and photogrammetric calibration.

The key to self calibration [2] is to find corresponding points in image sequences of static scenes. These correspondences are used to determine the internal and external camera parameters simultaneously.

The photogrammetric methods require control points with high geometrical precision that are captured from one or different viewpoints. These projected control points are extracted and identified to calculate the camera parameters. Multiple images are obligatory if the camera positions are not known accurately and a planar target is used. In this case it is not possible to determine the lines of sight for the imaged control points. If the corresponding lines of sight are available with high precision, all calibration parameters can be derived from a single view. Considering this fact, fixed stars are particularly suitable for calibration purposes, due to the high accuracy of their angular positions. Exploiting fixed stars as control points is not a new idea, although it is not established in the computer vision community so far. Schmid [9] proposed 1974 a stellar method to calibrate the Orbigon lens. More than 2400 stars are visible on each image plate, which have to be identified manually. Another necessity in this approach is the correction of the atmospheric refraction. In order to obtain the required accuracy, several observations are necessary to calculate a least square solution for the focal length, the principal point and the distortion parameters.

Gustavsson [4] presented an estimate of the three dimensional resolution of the Auroral Large Imaging System (ALIS), and discussed the sensitivity of the resolution to noise and artifacts. His work contains a chapter - geometrical calibration of ALIS - that presents a method to determine the orientation and optical characteristics of the used camera system. After manual identification of approximately 20 stars, the camera rotation and optical parameters are calculated. A subsequent semi-automatic step supports the search for more stars. Afterwards a final optimisation step is performed.

Much more research has been done at a related topic - the tracking of stars. Star trackers are used in autonomous attitude determination systems of spacecrafts. Such systems [1, 12] provide high precision attitude information in near-real time and consist of a digital camera that is mounted to the body of the spacecraft, a central processing unit and external memory for storing a star catalog. A segmentation step determines the sub-pixel position of the stars. In the following recognition step the identification of extracted stars is performed. This information is used to calculate the attitude with high precision.

*klaus@vrvis.at

In the following Sections 2 and 3 we explain the used camera model and give the astronomic fundamentals. Our calibration method is explained in Section 4. Experimental results are shown in Section 5. Finally, Section 6 presents the conclusions. For sake of clarity we denote stars which are extracted from the input image as luminaries, whereas stars from the star catalog are denoted as catalog stars.

2. Camera Model

Camera calibration is the task of solving the unknown parameters of the used camera model. Therefore we first have to define a camera model that fulfils our accuracy requirement. We use a projective camera model augmented with a common lens distortion correction [5]. Our camera model which projects the world coordinate $[X, Y, Z, 1]^T$ to the image coordinate $[x, y, 1]^T$ is given by

$$\lambda \begin{bmatrix} x \\ y \\ 1 \end{bmatrix} = \begin{bmatrix} s_x f & 0 & x_p & 0 \\ 0 & f & y_p & 0 \\ 0 & 0 & 1 & 0 \end{bmatrix} \begin{bmatrix} \mathbf{R} & \mathbf{t} \\ 0 & 1 \end{bmatrix} \begin{bmatrix} X \\ Y \\ Z \\ 1 \end{bmatrix},$$

where λ denotes an arbitrary scale factor, s_x the aspect ratio, f the focal length (in pixel), $cp = [x_p, y_p]^T$ the optical center (or principal point), $\mathbf{R}$ the rotation matrix and $\mathbf{t}$ the translation vector. Hence we have 6 degrees of freedom (DOF) for the extrinsic parameters $\mathbf{R}$ and $\mathbf{t}$ and 4 degrees for the remaining intrinsic parameters. The lens distortion is decomposed into a radial $\Delta r(a_d, k_1, k_2, ...)$ and a decentering $\Delta d(a_d, p_1, p_2, ...)$ component. The distorted image coordinates $\mathrm{a}_d = [x_d, y_d]^T$ and the corrected coordinates $\mathrm{a}_c = [x_c, y_c]^T$ are related by:

$$a_c = a_d + \Delta r(a_d, k_1, k_2, ...) + \Delta d(a_d, p_1, p_2, ...),$$

$$\Delta r(a_d, k_1, k_2, ...) = \begin{pmatrix} \overline{x}_d \\ \overline{y}_d \end{pmatrix} \sum_{i=1}^{\infty} k_i r_d^{2i},$$

$$\Delta d(a_d, p_1, p_2, ...) =$$

$$\begin{pmatrix} 2p_1\overline{x}_d\overline{y}_d + p_2(r_d^2 + 2\overline{x}_d^2) \\ p_1(r_d^2 + 2\overline{y}_d^2) + 2p_2\overline{x}_d\overline{y}_d \end{pmatrix} (1 + \sum_{i=1}^{\infty} p_{i+2} r_d^{2i})$$

where

$$\overline{x}_d = x_d - x_p, \overline{y}_d = y_d - y_p, r_d = \sqrt{(\overline{x}_d^2 + \overline{y}_d^2)}.$$

Higher order terms (i ≥ 3) of the radial distortion parameters k_i and the decentering distortion parameters p_i can be neglected, due to their insignificant relevance [5].

3. Basics of Astronomy

The most commonly used astronomical coordinate system to indicate the position of stars on the celestial sphere is the *equatorial coordinate system*. The *celestial sphere* is an imaginary sphere that represents the entire sky, with the observer located in its center. Spherical coordinates that are composed of three parameters (δ, α, r) can be used to indicate the object position in space, whereby the *declination* δ [-90° +90°] and the *right ascension* α [0h 24h] indicate its direction.

The *apparent magnitude* is a logarithmic measure of the brightness of a star as it appears to an observer on the earth and its unit is the magnitudo - one magnitudo is written as 1^m. Let m_1 and m_2 be two observed magnitudes and I_1 and I_2 their corresponding true intensities, then the following relation holds $m_1 - m_2 = -2.5 \cdot lg(I_1/I_2)$. With an unarmed eye it is possible to see stars with magnitudes less than 6^m. Sirius is the brightest star (except the sun) and has a magnitude of -1^m5. With a digital consumer camera and several seconds exposure time, stars of a magnitudo up to 20^m can be captured.

Next we address the effects caused by (i) parallax (ii) scintillation and (iii) refraction as the main sources for potential distortions in night sky imaging and discuss their relevance in our processing. The *parallax* of a (nearby) star is the angular displacement of the star against the background of more distant stars resulting from the motion of the earth in its orbit around the sun. With a distance of 3.26 light years, Proxima Centauri is the nearest fix star to our solar system and therefore its parallax of $0''762$ defines the upper limit for the expected parallaxes. Using a standard digital camera, the resulting pixel shift for a parallax of $1''$ is less than $1/50$ pixel and therefore negligible. The other effects make a luminary to appear as a disc rather than as a distinct point in the image, as it would be expected for point sources. First, quantum effects introduce diffraction. Second, turbulences in the atmosphere cause fluctuations in the magnitude and position of stars known as *scintillation*. These effects let luminaries to appear larger, which reduces the discriminatory of luminaries but, because of their radial symmetry, they do not change the centroid position of a single luminary.

Another important distortion that, in contrast to the others, has to be compensated explicitly is *refraction*. As any other physical medium also the atmosphere has a particular index of refraction that cause deflection of light rays which always seems to lift the luminaries and let them to appear closer to the zenith. The *zenith* is the point at which the celestial sphere is intersected by an upward extension of a plumb line from the observer's location on earth. While the refraction in the direction of the zenith is zero, it changes with an increasing difference angle θ to the zenith direction as a result of the earth's curvature. The effect can be compensated by a series of odd powers of tan-functions [10], thus

$$\theta_0(\theta) = \theta - 2.819676 \cdot 10^{-4} \cdot \tan(\theta) + \\ + 3.248252 \cdot 10^{-7} \cdot \tan^3(\theta) \quad (1)$$

denotes the corrected angle for an observed angle θ in radians. Considering a camera aligned with the zenith direction and an aperture angle of $50°$, the maximal shift caused by refraction can be determined to 0.017% of the image diagonal, i.e. the expected maximal shift using a 11 million pixel camera is about 0.858 pixel.

For a more detailed explanation of the above topics we refer to [8, 6]. In this paper we used the Yale Bright Star catalogue that contains the most important parameters, such as the declination, the right ascension and magnitudo, of approximately 32.000 stars.

4. The Stellar Calibration Method

Our calibration method is performed in three steps. First the stars in the image are extracted. As a result we obtain the image position and magnitude of the projected stars. In the second step an initial mapping between the extracted luminaries and the stars from the catalog is determined. In the last step a calibration parameter optimization and a consecutive mapping rectification are repeated several times.

4.1. Sky Segmentation and Star Centroiding

From the simple observation that a star is mapped to an image as a bright region on dark background, the segmentation of stars is easily done by binarization of the image using a percentile threshold. Due to illumination differences, which primarily stem from lens vignetting, distinct block processing is used to obtain a robust star segmentation and to ensure uniform distributed luminaries over the whole image. Small regions, which usually correspond to pixel defects, like hot pixel defects, are discarded. The segmentation yields coarse coordinates of the luminary centroids.

The refinement of the center position of a star is shown in Figure 1. The surrounding patch of size 15×15 pixels (Figure 1(a)), is upsampled by a given factor (Figure 1(c)) and the corresponding gradient map is calculated (Figure 1(d)). Starting from the brightest region, the gray value threshold is decreased, until an energy function is maximized. The energy function is defined as the sum of the border gradients and normalized by the border length (Figure 1(e)). This leads to a segmented star image shown in Figure 1(f). The segmentation ensures that the weighted center of gravity algorithm [11] gives a robust estimation. Furthermore weighted centering leads to more accurate results than using only binary weight centering.

The proposed method of centroid finding gives robust results even in noisy images, which is the case in night sky imaging. The magnitude of a luminary is calculated as the sum of the segmented gray values, so that a small but bright star gets a higher magnitude than a large dark one.

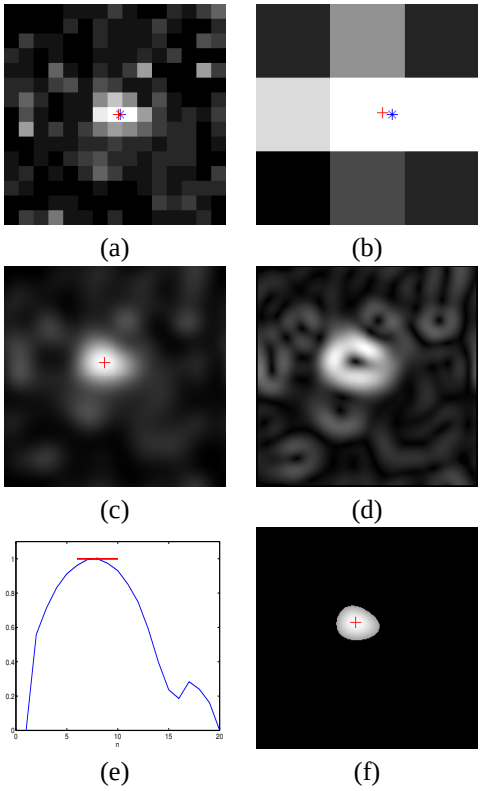

Figure 1: Centroid estimation: star '*' indicates the initial solution and cross '+' gives the optimized solution (a) 15×15 pixel star neighborhood, (b) zoom of the center 3×3 pixels, (c) patch upsampled by a factor of 2^4, (d) gradient map, (e) energy function with shown maximum (f) segmented star.

4.2. Initial Estimation and Initial Mapping

Once we have extracted the position and magnitude of the luminaries, an initial estimation of the essential camera parameters can be achieved. Star tracking systems use precalibrated cameras and therefore have to solve the camera rotation only. This task is significantly simpler than our case, where the focal length is an additional DOF. Also problematic is the unknown lens distortion which, according to the lens, can cause a high distortion at border regions of the image (size of several hundred pixels). Nevertheless it is possible to determine the essential parameters efficiently by using a RANSAC [3] like procedure. If we have an arbitrary mapping between two luminaries and two stars in the catalog, it is possible to solve 4 DOF. Hence, the orientation (3 DOF) and the focal length can be determined for this mapping. In order to find correct mappings, a quite

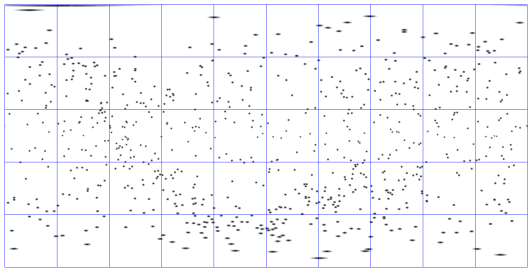

Figure 2: Star map for distance transformation containing the brightest 800 stars. Stars close to the poles are distorted due to the regular mapping.

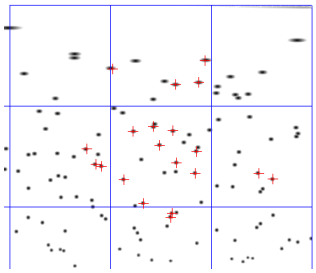

Figure 3: A correct mapping between the extracted luminaries and the map stars implicates a high score. In this example all extracted stars, indicated by crosses, have been found in the map.

high number of combinations have to be verified. All mappings are rated using the remaining stars. If the essential camera parameters are determined by correct mappings, the projected stars from the star catalog are close to corresponding candidates. The best mapping maximizes the number of candidates that are within a given threshold. In order to reach high performance only probable combinations are verified very efficiently using the star map in Figure 2. Since we ignore lens distortion in this step, we are only using stars extracted close to the camera center. Our procedure to find a initial estimate is as follows:

1: Select the n_i brightest luminaries $S_I = \{l_1 ... l_{ni}\}$ with a quite small distance d_i to the image center (good values empirically found are $n_i = 20$ and $d_i = imagediagonal/4$)
2: Select the n_c brightest catalog stars $S_C = \{s_1 ... s_{nc}\}$ (a sufficient large value is $n_c = 100$)
3: **for all** $\{(l_i, l_j) | l_i, l_j \in S_I; i < j\}$ **do**
4: **for all** $\{(s_i, s_j) | s_i, s_j \in S_C; i < j\}$ **do**
5: Calculate camera rotation and focal length
6: Determine a score for current mapping by calculating spherical coordinates for the remaining $n_i - 2$ stars and perform a star map look up as illustrated in Figure 3
7: **if** score is new maximum **then**
8: store current parameters
9: **end if**
10: **end for**
11: **end for**
12: **if** score is too low (less than 50% of stars found in map) **then**
13: Double n_c and go to 1 (proceed search for better mapping)
14: **end if**

4.3. Parameter Optimization

So far we have found a good estimate of the camera rotation and the focal length. The remaining parameters are initially set to default values. The distortion coefficients are set to zero, the principal point to the image center and the aspect ratio to one. The optimization of the unknown parameters and the refinement of the estimated ones is challenging, since it depends on a correct mapping and vice versa. We solve this problem iteratively, where in each iteration a new mapping with successive non-linear optimization is performed. In order to ensure a fast convergence, we use a decreasing threshold to truncate the maximum cost of each correspondence.

Mapping for Current Parameters The task of the mapping step is to find the nearest n_{map} candidates for the brightest catalog stars within the camera frustum. This is done as follows:

1: **for all** stars of the star catalog (sorted according to their brightness) **do**
2: Displace star to emulate atmospheric refraction by formula 1
3: **if** displaced star is in camera frustum **then**
4: Project displaced star into image using current camera and distortion parameters
5: Use kd-tree data structure for efficient nearest neighbor query
6: **if** distance is below threshold **then**
7: Append assignment (c_{ind}, l_{ind}) to the current mapping M_{CL}, where c_{ind} indicates the index of the catalog star and l_{ind} of the luminary
8: **end if**
9: **if** n_{map} stars are in camera frustum **then**
10: exit
11: **end if**
12: **end if**
13: **end for**

The number n_{map} is derived from the number of extracted luminaries n_{ext} . In order to enable faster convergence, n_{map} should be smaller than n_{ext}, as this increases the probability that a correct correspondence exists. A good

ratio that has been found empirically is $n_{map} = 0.75 n_{ext}$. In order to incorporate the atmospheric refraction the zenith direction of the exposure position is required. There are three possibilities to determine the unknown two angles: (i) The zenith direction can be derived from the camera direction as well as exposure date and exposure position (longitude and latitude). (ii) The camera is assumed to be aligned to the zenith direction. The direction is determined by the line of sight that goes through the principal point. (iii) The zenith direction is solved as two additional DOF in the optimization step. For the initialization the line of sight through the principal point is used as before. Since we do not require any user input, our method uses this procedure.

Levenberg-Marquardt Optimization The found mapping $M_{CL} = \{m_1 ... m_{msize}\}$ enables the refinement of all parameters. A particularly qualified optimization method is the Levenberg-Marquardt algorithm [7], which is a general non-linear minimization algorithm. It dynamically mixes Gauss-Newton and gradient-descent iterations and provides fast convergence. As a result we receive the optimized parameters, which minimize the sum of squared distances between the projected catalog stars c_{proj} and the corresponding extracted luminaries l_{ext} for the current mapping:

$$\sum_{i=1}^{msize} |c_{proj}[m_i \rightarrow c_{ind}] - l_{ext}[m_i \rightarrow c_{ind}]|^2 \longrightarrow min$$

5. Experimental Results

Images from several digital consumer cameras are used to analyze our calibration method in terms of robustness, accuracy and performance. The results are shown in Table 1. The calibration succeeded for all cameras. The exposure time ranges between 10 and 30 seconds. One problem occurred for the image captured with the Olympus camera. The original method determined a wrong initial solution for the telephoto image, due to too few stars of the star map that were located within the camera frustum. The problem was solved by increasing the number of stars from 800 to 2000.

The mean error between projected stars and corresponding luminaries ranges between 0.129 and 0.21 pixels and is mainly caused by the inaccuracy of the star centroiding. In the Figures 6 to 9 the calibration results are displayed using different diagrams. In the upper diagram the determined polynomial for the radial distortion is plotted. The middle diagram shows an error distribution of the radial distance from the principal point. The stars of the determined mapping are indicated by crosses. In the lower left, an error histogram is displayed. In the lower right, the two-dimensional error between the projected stars and the corresponding luminaries is shown.

The precision of finding the centroid of an object depends on its size and on its contrast to the background. Thus, the precision decreases for darker stars as shown in Figure 4. We selected approximately 2100 luminaries that were contained in the mapping of two different Canon 1Ds images. They were sorted according to their magnitude and combined in pins. The mean error of each block is used to illustrate the dependency between brightness and accuracy.

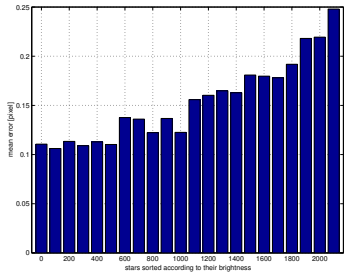

Figure 4: The accuracy of the star centroiding depends on the brightness of the stars. The mean error increases for darker stars.

Figure 5: The vertical vanishing point is calculated using the extracted vertical lines of the house (zoomed out). It serves as reference value for the determined zenith direction which intersects the image plane at the position indicated by the left dot.

Experiments show that a wrong zenith direction causes only a very small error. Two reasons are responsible for this effect: First the effect of the atmospheric refraction is low and second the aberration caused by a wrong direction is compensated through the other camera parameters. These facts can interfere the correct determination. Therefore an experiment was performed to evaluate the calculated direction of the zenith. We captured an image (Figure 5) containing the night sky as well as a part of a house. We resampled the image to compensate the lens distortion, extracted lines and used them to calculate the vertical vanishing point. From this vanishing point the zenith direction was derived and used as reference value. The image coordinate of the

Camera & Objective	*used image format*	*radial distortion k1-k3*	*decentering distortion p1,p2*	*principal point*	*focal length [pixel]*	*aspect ratio*	*number of correspondences*	*mean error [pixel]*	*calculation time [sec] on Athlon 2200+*	*figure*
Canon 1Ds & Sigma EX [15mm]	4064∗2704	+3.386e-08 +4.294e-15 +6.739e-22	-1.770e-07 +6.688e-08	2058.789 1348.953	1763.798	0.9997	859	0.133	50.9	6
Canon 1Ds & Sigma EX [30mm]	4064∗2704	-5.656e-10 -1.188e-15 +4.384e-24	-1.142e-07 +1.118e-07	2051.640 1351.964	3290.615	0.9999	678	0.129	78.9	7
Minolta Dimage 7i	2560∗1920	+3.939e-08 -3.981e-15 -7.423e-23	-4.746e-07 -3.709e-07	1265.785 908.248	2177.894	0.9998	866	0.193	87.6	8
FujiFilm S1 & Tamron 28-105	800∗600	-2.176e-07 -7.212e-12 -5.575e-18	+2.764e-07 -1.185e-07	404.104 251.380	1603.525	0.9997	420	0.165	28.2	9
Olympus E-10	2240∗1680	-2.066e-08 -7.948e-14 -1.199e-20	+1.025e-07 -9.532-07	1243.597 820.915	9092.184	0.9983	119	0.21	83.2	/

Table 1: Camera calibration results for images captured with several cameras.

determined vanishing point is $[1914, -612]^T$, whereas the zenith direction determined in our calibration method intersects the image plane at $[1718, -629]^T$. Considering the parameters of the used camera (Canon 1Ds with Sigma lens [15mm]) the angle between the corresponding lines of sight can be calculated. It is approximately 3.1 degrees - a deviation with a very low impact (less than 1/400 for the camera considered in Section 3) since the direction is only used to incorporate the atmospheric refraction.

6. Summary and Conclusions

We have developed a universal camera calibration method that performs well in terms of accuracy, robustness and performance. In contrast to classical techniques which use a 2D calibration target, the proposed method enables the determination of all essential camera and distortion parameters from a single input image. Other techniques which require extensive setups such as two or three orthogonal targets are outperformed in terms of costs and flexibility. Our method works with night sky images captured anywhere all over the world and enables remote calibration. We plan to offer our camera calibration as a service. For more information, visit *www.vrvis.at/CameraCalibration*.

Acknowledgments

Parts of this work have been done in the VRVis research center, Graz and Vienna/Austria (http://www.vrvis.at), which is partly funded by the Austrian government research program Kplus. Horst Bischof acknowledges the support of the Kplus competence center Advanced Computer Vision (ACV) funded by the Kplus program.

References

[1] T. Bak and R. Wisniewski and M. Blanke, Autonomous attitude determination and control system for the rsted satellite, *In IEEE Aerospace Applications Conference*, February 1996.

[2] O.D. Faugeras and Q.T. Luong and S.-J. Maybank, Camera Self-Calibration: Theory and Experiments, *European Conference on Computer Vision*, pp. 321-334, 1992.

[3] M. Fischler and R. Bolles, Random sample consensus: A paradigm for model fitting with applications to image analysis and automated cartography, *Communications of the Association for Computing Machinery*, Vol. 22, Nr. 24(6), pp. 381-395, 1981.

[4] B. Gustavsson, *Three dimensional imaging of aurora and airglow*, PhD thesis, 2000.

[5] J. Heikkilä, Geometric Camera Calibration Using Circular Control Points, *IEEE Transactions on Pattern Analysis and Machine Intelligence*, Vol. 22, Nr. 10, pp. 1066-1077, 2000.

[6] H.-U. Keller, *Astrowissen*, Franckh-Kosmos Verlags GmbH & Co, Stuttgart, 1994.

[7] J.J. Mor, *The Levenberg-Marquardt Algorithm: Implementation and Theory*, Springer-Verlag, 1977.

[8] G.D. Roth, *Handbuch für Sternenfreunde*, Springer-Verlag, 1981.

[9] H.H. Schmid, Stellar calibration of the orbigon lens, *Photogrammetric Engineering*, 40(1), pp. 101-111, 1974.

[10] W.M. Smart, *Textbook on Spherical Astronomy*, $6^{th} edition$, Cambridge University Press, 1977.

[11] E.W. Weisstein, Geometric Centroid, *Eric Weisstein's World of Mathematics. http://mathworld.wolfram.com/GeometricCentroid.html*, 1999-2003.

[12] R. Wisniewski and M. Blank, Three-axis Satellite Attitude Control Based on Magnetic Torquing, *13th IFAC World Congress*, June 1996.

[13] Z. Zhang, A Flexible New Technique for Camera Calibration, *IEEE Transactions on Pattern Analysis and Machine Intelligence*, Vol. 22, Nr. 11, pp. 1330-1334, 2000.

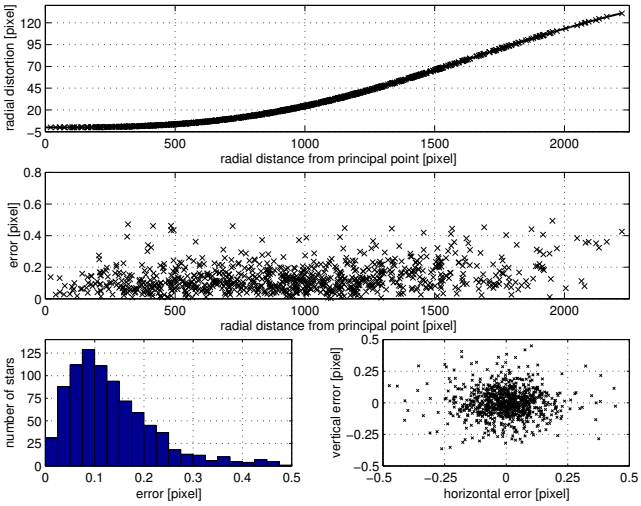

Figure 6: Calibration results for Canon EOS-1Ds with Sigma EX 15-30mm [15mm]

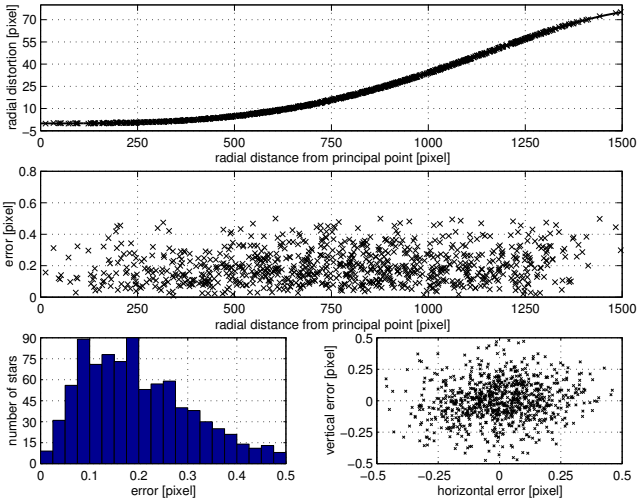

Figure 8: Calibration results for Minolta Dimage 7i

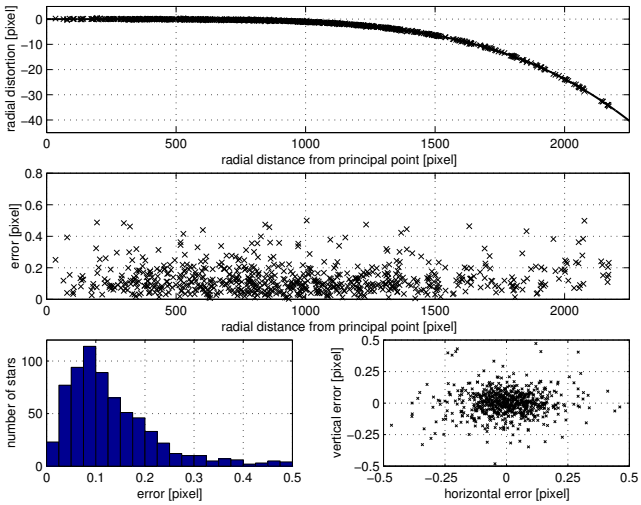

Figure 7: Calibration results for Canon EOS-1Ds with Sigma EX 15-30mm [30mm]

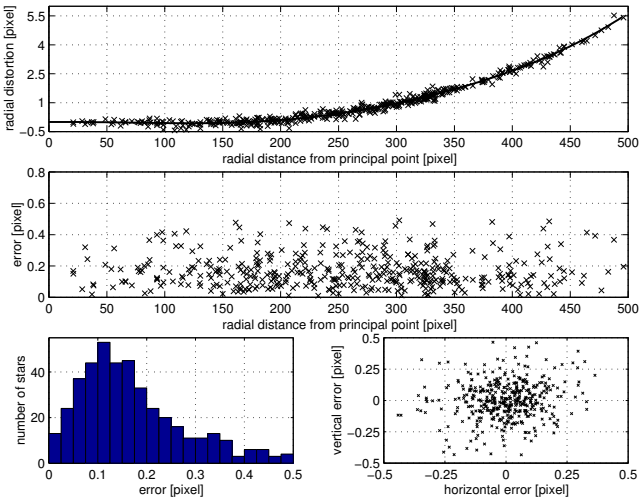

Figure 9: Calibration results for FujiFilm FinePix S1 with Tamron 28-105